

Characterization of model bile using fluorescence energy transfer from dehydroergosterol to dansylated lecithin

Steven P. Wrenn,^{1,*} Manasa Gudheti,^{*} Anka N. Veleva,[†] Eric W. Kaler,[†] and Sum P. Lee[§]

Chemical Engineering Department,^{*} Drexel University, Philadelphia, PA 19104; Center for Molecular and Engineering Thermodynamics,[†] Department of Chemical Engineering, University of Delaware, Newark, DE 19716; and University of Washington School of Medicine,[§] Seattle, WA. 98195

Abstract Fluorescence energy transfer from dehydroergosterol (DHE) to dansylated lecithin (DL) was used to characterize lecithin-cholesterol vesicles in the presence of the bile salt, sodium taurocholate. At lipid concentrations approximating physiological levels, exposure of fluorescently labeled vesicles to the bile salt led to a dose-dependent increase in the DHE-to-DL fluorescence ratio during the first 24 h after mixing. The initial changes in the fluorescence ratio correlated well with conventional turbidity measurements that quantify partial micellization of vesicles as a function of bile salt loading. In addition, fluorescence energy transfer from DHE to DL revealed cholesterol enrichment of vesicles and re-vesiculation of micelles at bile salt loadings for which vesicles and micelles coexisted. Samples containing the cholesterol-enriched vesicle fraction exhibited further increases in the DHE-to-DL fluorescence ratio during a 4-week observation period but only after a significant lag period of several days. The lag period decreased with cholesterol loading, and the increase in the fluorescence ratio always preceded the appearance of microscopic, birefringent, either needlelike or platelike, cholesterol crystals, in samples that were initially supersaturated with cholesterol. Cholesterol crystals were not observed, and the fluorescence ratio did not increase, for any sample that was undersaturated with cholesterol. Taken together, these results suggest that the latter changes in fluorescence are the result of cholesterol nucleation. Fluorescence energy transfer from DHE to DL is therefore a promising technique for the characterization of model bile and, possibly, provides a direct measurement of cholesterol nucleation.—Wrenn, S. P., M. Gudheti, A. N. Veleva, E. W. Kaler, and S. P. Lee. **Characterization of model bile using fluorescence energy transfer from dehydroergosterol to dansylated lecithin** *J. Lipid Res.* 2001. 42: 923–934.

Supplementary key words gallstones • bile • micelles • phospholipids • crystals

Cholesterol supersaturation in bile is a prerequisite for gallstone formation, but cholesterol supersaturation alone cannot predict the occurrence of stones (1). The critical factor in gallstone pathogenesis is the rate at which dissolved cholesterol nucleates into cholesterol monohydrate crystals, the precursors to stones (2). Despite the recognition of this fact nearly two decades ago, little is known about the choles-

terol nucleation mechanism in bile (3). Gallstone formation begins with the hepatic secretion of metastable lecithin-cholesterol vesicles (4). The vesicles encounter bile salts, which are secreted by the liver via a separate pathway, as they travel to the gallbladder (5). A vesicle-to-micelle transition ensues, giving rise to bile salt-lecithin-cholesterol mixed micelles, but micellization is incomplete and favors the transport of lecithin relative to cholesterol (6). Lecithin-cholesterol vesicles therefore remain in the gallbladder and are cholesterol-enriched relative to the hepatic vesicles.

Cholesterol that nucleates comes from the cholesterol-enriched vesicles (7). Whereas mixed micelles are thermodynamically stable, vesicles are metastable and eventually revert to a lamellar phase at equilibrium. If the cholesterol-to-lecithin molar ratio (Ch:L) of the cholesterol-enriched vesicles exceeds unity, then attainment of equilibrium yields cholesterol monohydrate crystals as an additional phase (8); however, gallstone formation requires nucleation of the excess cholesterol during the short residence time of bile within the biliary tract.

The rate at which vesicles nucleate excess cholesterol varies with the Ch:L ratio of the vesicles and with the total lipids concentration (9). Bile salt composition is an important physiological factor because the cholesterol-solubilizing capacity of the mixed micelle sets the number density and the Ch:L ratio of vesicles, and one thus expects the rate of cholesterol nucleation to vary with bile salt hydrophobicity. The problem becomes complicated in native bile, however, owing to a variety of physiological factors. Numerous studies confirm the existence of pro- and anti-nucleating proteins that enhance or inhibit cholesterol nucleation, respectively (10–13). As with nucle-

Abbreviations: L, egg yolk lecithin; CH, cholesterol; DHE, dehydroergosterol; DL, dansylated lecithin, or 1-(O-(11-(5-dimethylamino)naphthalene-1-sulfonyl)amino)undecyl)-2-decanoyl-sn-glycero-3-phosphocholine; NaTC, sodium taurocholate.

¹ To whom correspondence should be addressed at Drexel University, Chemical Engineering Department, 3141 Chestnut Street—CAT Bldg., Philadelphia, PA 19104.

e-mail: wrenn@coe.drexel.edu

ation itself, the mechanisms by which the various proteins influence the rate of nucleation are unknown.

Acquiring the desired mechanistic information requires an analytical tool that allows direct measurement of the cholesterol nucleation event. No such tool has materialized, and most nucleation studies characterize the kinetic factors in bile according to a "nucleation time" (3, 14–16). The method records the time for cholesterol crystals to become visible with an optical microscope and provides no information about nucleation kinetics (17, 18). Recent attempts to quantify nucleation involve generation of a crystal growth curve from turbidity measurements (13, 19). Although the turbidity technique improves on the nucleation time method because it provides the entire crystal growth curve rather than a single point, neither technique measures the first molecular scale events of nucleation. Because they do not detect or quantify nucleation, these methods are more appropriately referred to as "crystal appearance time" assays.

The molecular events of nucleation begin with the random clustering of cholesterol molecules within the vesicle bilayer. Stable cholesterol nuclei result when randomly formed clusters exceed a critical size, and nucleation occurs when these nuclei exit (i.e., nucleate from) the vesicle and coalesce into a microcrystalline phase. The process of nucleation continually removes cholesterol from the lecithin-cholesterol vesicles and delivers cholesterol to the nascent crystalline phase, which grows and eventually produces macroscopic cholesterol monohydrate crystals. Therefore, an analytical method that is sensitive to the separation between cholesterol and lecithin offers the possibility of measuring cholesterol nucleation at the molecular level.

An ideal candidate is fluorescence energy transfer from dehydroergosterol (DHE) to dansylated lecithin (DL), since the efficiency of energy transfer depends heavily ($1/r^6$) on the separation, r , between fluorophores (20). If both DHE and DL reside in the vesicle bilayer, the extent of energy transfer will be large and give rise to a low DHE fluorescence signal. Any process that separates DHE from DL should alleviate energy transfer and lead to a measurable increase in the DHE fluorescence intensity. One such process is nucleation of DHE, which is known to co-crystallize with cholesterol (21), into the nascent crystalline phase and the concomitant separation from the DL that remains in the vesicle bilayer.

We recently reported (22) the use of DHE-to-DL energy transfer to characterize lecithin-cholesterol vesicles in the presence of the pro-nucleating enzyme, phospholipase C. In the current study we extend the fluorescence technique to investigate lecithin-cholesterol vesicles in the presence of the bile salt, sodium taurocholate (NaTC). Our approach is to first demonstrate agreement between the new fluorescence technique and conventional studies with respect to the vesicle-to-micelle transition as a function of bile salt loading. We then explore the possibility of using energy transfer from DHE to DL as an assay for measuring cholesterol nucleation. The mixing of vesicles with NaTC in this study mimics the action in the biliary tract, and the model bile solutions utilized herein approximate physiological lipid concentrations.

MATERIALS AND METHODS

Materials

Egg yolk lecithin (L), CH, and DHE, all of analytical grade, were purchased from Sigma (St. Louis, MO) and used without further purification. NaTC of highest purity (Ultral Grade) was purchased from Calbiochem (La Jolla, CA), and 1-(O-(11-(5-dimethylamino)naphthalene-1-sulfonyl)amino)undecyl)-2-decanoyl-sn-glycero-3-phosphocholine (DL) was purchased from Molecular Probes (Eugene, OR).

Vesicle preparation

Mixtures of CH, L, DHE, and DL were co-precipitated from chloroform/MeOH (90/10 v/v) solutions to give lipid films of desired composition. DHE accounted for 15 or 17.5 mol% of the total sterol, and DL comprised 4.5 mole% of the total lecithin. Films were hydrated with an aqueous buffer solution (0.15 M NaCl, 5 mM CaCl₂, 5 mM HEPES, and 0.02 wt % NaN₃, pH = 7.4) and were sonicated in the direct mode for 90 min (Heat Systems Ultrasonics Model W-225). An ice/water bath and a nitrogen blanket were used to prevent lipid degradation during sonication, and the resulting bluish dispersions were centrifuged for 2 h at 32,000 g and 25°C (DuPont Sorval RB). The supernatant was diluted with buffer solution as necessary to give unilamellar vesicles at the desired concentration.

Model bile solutions

Three sets of model bile solutions were used. In all cases, model bile was prepared by adding vesicles to an aqueous solution of NaTC, prepared in buffer with rapid mixing. The first set (set A) constituted a cut through the triangular lecithin-sterol-NaTC composition space at a fixed sterol-to-lecithin molar ratio of 1.32, and all samples in this set were prepared by adding 1 ml of a vesicle solution into 2 ml of an NaTC solution. A single vesicle solution was used, and the final number density of vesicles was identical in all samples. Different NaTC solutions were used, which varied in concentration from 0 to 130 mM, and the corresponding total solids concentration ranged from 0.13 to 4.81 g/dl. **Table 1** gives the properties of the model biles in set A (samples A1–A16).

A second set (B) of model biles was prepared in the same way as the first but with a sterol-to-lecithin molar ratio of 1.22. The samples in this set were observed over a period of 4 weeks, and duplicate samples were made to allow microscopic observations without disturbing the samples used for fluorescence and turbidity analyses. **Table 1** summarizes the model biles in this set, denoted as B1–B7.

The third set (C) of model biles comprised five samples (C1–C5), each with a total solids concentration of 2.29 g/dl and a mole fraction of lecithin (L plus DL), on a sterol-free basis, of 0.028. The samples differed with respect to the ratio of sterol to lecithin in the starting vesicles, and this set constituted a cut through the lecithin-sterol-NaTC composition space at a fixed lecithin-to-NaTC molar ratio. Five vesicle solutions were prepared in set C that contained varying amounts of sterol and lecithin. Reaching the same total solids content in each sample required mixing approximately 1 ml of each vesicle solution with approximately 2 ml of a nominally 60 mM NaTC solution. **Table 2** gives the sterol-to-lecithin ratios of the vesicle solutions, the concentrations of the NaTC solutions, and the compositions of the resulting model biles in set C.

Analysis of model biles

Turbidity and fluorescence measurements were performed on the three model bile sets using a Perkin Elmer Lambda 2 absorbance spectrophotometer and an SLM Aminco 8100 fluorescence spectrophotometer, respectively. Set A was examined for 24 h, and sets B and C were monitored for 4 weeks. Crystal appearance

TABLE 1. Model bile solutions with fixed sterol-to-lecithin molar ratios

Sample	[NaTC]	Total	Ch:L ^b	L(L+NaTC) ^c	CHOL	DHE	LEC	DL	NaTC
	<i>mM^a</i>	<i>g/dL</i>					<i>mol%</i>		
A1	0	0.13	1.32	1.000	48.32	8.60	41.16	1.92	0.00
A2	3	0.25	1.32	0.326	25.56	4.55	21.77	1.02	47.10
A3	5	0.31	1.32	0.239	20.39	3.63	17.37	0.81	57.80
A4	8	0.40	1.32	0.173	15.82	2.82	13.47	0.63	67.26
A5	10	0.49	1.32	0.136	12.92	2.30	11.01	0.51	73.26
A6	20	0.85	1.32	0.073	7.46	1.33	6.35	0.30	84.57
A7	30	1.21	1.32	0.050	5.24	0.93	4.46	0.21	89.15
A8	35	1.39	1.32	0.043	4.56	0.81	3.89	0.18	90.56
A9	40	1.57	1.32	0.038	4.04	0.72	3.44	0.16	91.64
A10	45	1.75	1.32	0.034	3.63	0.65	3.09	0.14	92.50
A11	50	1.93	1.32	0.030	3.29	0.59	2.80	0.13	93.20
A12	60	2.29	1.32	0.026	2.77	0.49	2.36	0.11	94.27
A13	70	2.65	1.32	0.022	2.39	0.43	2.04	0.10	95.04
A14	85	3.19	1.32	0.018	1.99	0.35	1.69	0.08	95.88
A15	100	3.73	1.32	0.015	1.70	0.30	1.45	0.07	96.48
A16	130	4.81	1.32	0.012	1.32	0.23	1.12	0.05	97.27
B1	0	0.14	1.22	1.000	45.40	9.63	42.73	2.24	0.00
B2	10	0.50	1.22	0.146	12.50	2.65	11.76	0.62	72.47
B3	40	1.57	1.22	0.041	3.94	0.83	3.70	0.19	91.33
B4	60	2.29	1.22	0.028	2.71	0.57	2.55	0.13	94.04
B5	80	3.01	1.22	0.021	2.06	0.44	1.94	0.10	95.47
B6	100	3.73	1.22	0.017	1.66	0.35	1.56	0.08	96.34
B7	150	5.52	1.22	0.011	1.12	0.24	1.06	0.06	97.53

^aInitial NaTC concentration, prior to mixing with vesicles.

^bMolar ratio of total sterols (Chol + DHE) to total lecithins (Lec + DL); values apply to starting vesicles and final model biles.

^cSterol-free mole fraction of total lecithins (L includes Lec + DL).

times in the set B and set C samples were determined by observation in a Leica optical microscope. Crystal appearance time was defined as the time required for birefringent, either needlelike or platelike, crystals to become visible in the microscope at a magnification of 400×. All experiments were performed at room temperature, and samples were maintained under a nitrogen atmosphere to prevent lipid oxidation.

Dynamic light scattering

All light-scattering measurements were performed using a Brookhaven 90Plus particle size analyzer. This system consists of a 15-mW, solid state laser operating at a 688-nm wavelength and a BI-9000AT digital autocorrelator. The measured autocorrelation functions were analyzed for the first and second cumulants of a cumulant fit, which provide measures of the apparent diffusivity and the polydispersity, respectively. The data are given in terms of an effective diameter using the Stokes-Einstein equation

$$\text{Effective diameter} = k_B T / 3\pi\eta D \quad \text{Eq. 1}$$

where k_B is the Boltzmann constant, T is the temperature (25°), η is the solvent viscosity, and D is the diffusivity from the first cumulant.

Gel filtration studies

Several samples with concentrations and compositions matching those of model bile set A were fractionated on a Sephadex G75 gel column. The column was prepared with an aqueous buffer solution that contained 7.5 mM NaTC to approximate the bile salt inter-micellar concentration (IMC). The column was eluted at a rate of ~1 ml/min, and fractions were collected in 3-ml increments for characterization by dynamic light scattering and turbidity.

Volumetric mixing of fluorescently labeled vesicles and micelles

In a separate study, vesicles with a composition matching A1 were prepared by the customary sonication procedure. A separate, fluorescently labeled micellar sample was prepared by coprecipitating CH, L, DHE, and DL to yield a lipid mixture with the same composition as sample A16. This sample was not sonicated but was dissolved directly in an NaTC buffer solution to yield an isotropic solution of micelles. Fluorescently labeled vesicles and fluorescently labeled micelles were then mixed to varying extents to yield solutions containing 0%, 25%, 50%, 75%, and 100% micelles, on a volume basis. The fluorescence spectra

TABLE 2. Model bile solutions with fixed lecithin-to-NaTC molar ratios

Sample	[NaTC]	Total	Ch:L ^b	L(L+NaTC) ^c	CHOL	DHE	LEC	DL	NaTC
	<i>mM^a</i>	<i>g/dL</i>					<i>mol%</i>		
C1	55	2.29	0.49	0.028	1.11	0.24	2.59	0.14	95.92
C2	58	2.29	1.00	0.028	2.23	0.47	2.56	0.14	94.60
C3	60	2.29	1.22	0.028	2.71	0.57	2.55	0.13	94.04
C4	62	2.29	1.50	0.028	3.29	0.70	2.53	0.13	93.35
C5	65	2.29	1.86	0.028	4.04	0.86	2.5	0.13	92.47

^aInitial NaTC concentration, prior to mixing with vesicles.

^bMolar ratio of total sterols (Chol + DHE) to total lecithins (Lec + DL); values apply to starting vesicles and final model biles.

^cSterol-free mole fraction of total lecithins (L includes Lec + DL).

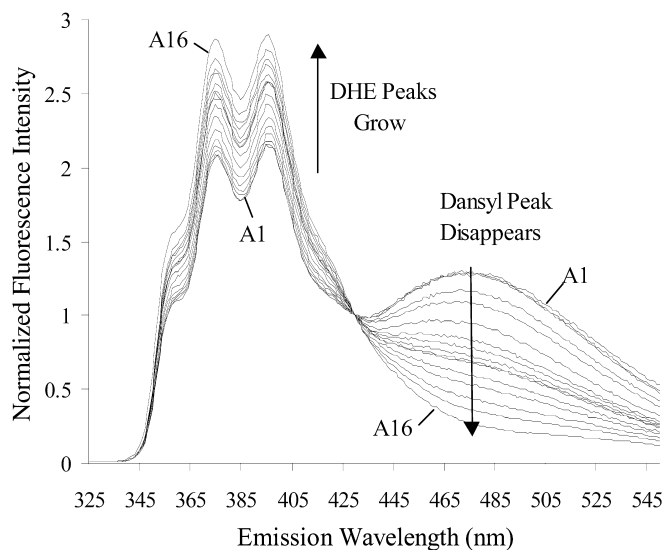


Fig. 1. The effect of mixing lecithin-cholesterol vesicles, labeled with DHE and DL, with varying amounts of NaTC is shown. Fluorescence emission spectra are plotted for the 16 model bile samples that make up set A. Spectral peaks at 355, 373, and 393 nm correspond to DHE, and a dansyl emission maximum occurs at 475 nm. In the absence of NaTC, DHE-to-DL energy transfer proceeds readily so that the smallest DHE peaks and largest dansyl peak occur in sample A1. The addition of NaTC alleviates energy transfer; the DHE fluorescence peaks grow, and the dansyl peak concomitantly and progressively decreases from sample A1 to A16. Excitation was at 300 nm, and fluorescence intensities were normalized at 430 nm.

of these mixtures were measured on a PTI, Inc. A1070 fluorescence spectrophotometer.

RESULTS

Model biles—set A

Figure 1 shows the fluorescence emission spectra of the model bile samples in set A immediately after mixing the vesicles with NaTC.² DHE exhibits three emission maxima at 355, 373, and 393 nm, and DL exhibits a single emission maximum at 475 nm. The samples were excited at 300 nm, a wavelength at which dansyl does not absorb strongly, and the DL fluorescence is due primarily to energy transfer from DHE. Energy transfer proceeds readily in the absence of NaTC, and both the smallest DHE peak and maximal DL peak occur in sample A1.

The addition of NaTC alleviates energy transfer, and increasing the concentration of NaTC in data set A induces growth of the DHE spectral peaks and decreases the intensity of the DL emission maximum. The trends of increasing DHE intensity and decreasing DL intensity follow the progression of samples from A1 to A16, and sample A16 gives both the maximal DHE fluorescence intensity and the minimal DL emission intensity. It is suspected that the alleviation of energy transfer in **Fig. 1** results from micellization of the vesicles.

² The experiments described herein have been repeated several times with excellent reproducibility. The data and figures are from individual, but typical, experiments.

To test this hypothesis, a control experiment was performed in which fluorescently labeled vesicles (effective diameter = 116 nm) and fluorescently labeled micelles (effective diameter ~9 nm) were prepared separately and mixed in varying proportions. **Figure 2** shows the fluorescence spectra for the individual vesicles and micelles, along with three mixtures that contained different amounts of the two particles. It is seen that increasing the micellar fraction yields both an increase in DHE fluorescence intensity and a decrease in DL fluorescence intensity, similar to the results of **Fig. 1**. Moreover, no energy transfer from DHE to DL is observed for the purely micellar sample in **Fig. 2**.

Careful inspection of **Fig. 1** reveals a slight DL blue shift as a function of NaTC loading. The blue shift is more pronounced 24 h after mixing, and **Fig. 3** gives the 24-h DL emission wavelength as a function of NaTC concentration. Included in **Fig. 3** are the emission wavelengths corresponding to maximal DL fluorescence intensities (henceforth referred to as *maximal DL emission wavelengths*), obtained 24 h after mixing, when samples A1–A16 were excited at 380 nm. DHE does not absorb at this wavelength, and 380-nm light excites DL alone. **Fig. 3** therefore compares direct dansyl excitation at 380 nm with the indirect excitation that is achieved via DHE-to-DL energy transfer at 300 nm.

No change in the maximal DL emission wavelength occurs, regardless of excitation wavelength, until an NaTC loading of 3 mM. At concentrations between 3 and 30 mM NaTC, indirect excitation yields a 20-nm decrease in the DL emission wavelength. Indirect excitation yields no fur-

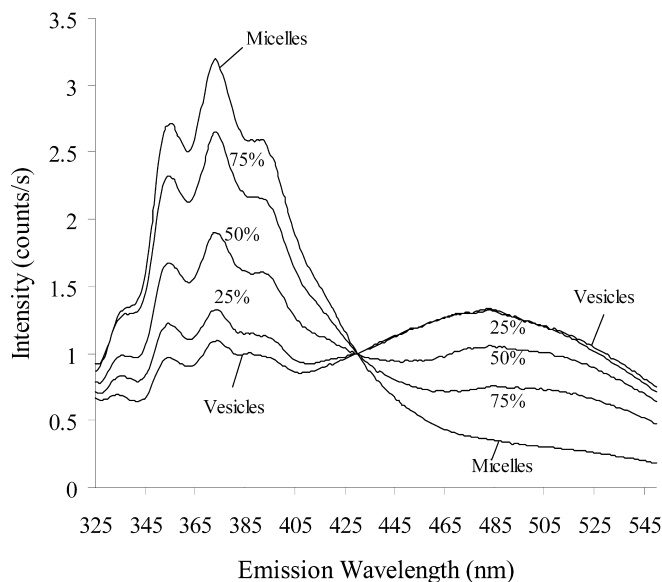


Fig. 2. The effect of mixing varying proportions of fluorescently labeled vesicles and fluorescently labeled micelles is shown. Vesicles were prepared by sonication of a lipid mixture with a composition identical to sample A1. Micelles were prepared by direct dissolution of lipids in 200 mM NaTC, in which the lipid composition matched that of sample A16. Vesicles and micelles were mixed to give samples containing 25%, 50%, and 75% micelles (volume basis). Excitation was at 300 nm, and fluorescence intensities were normalized at an emission wavelength of 430 nm.

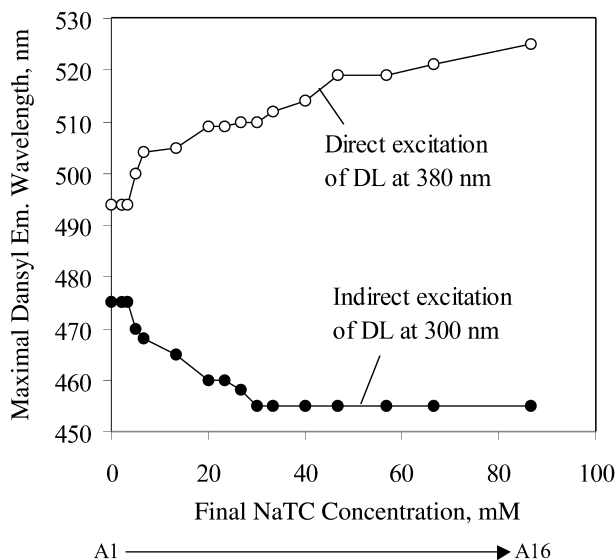


Fig. 3. The maximal DL emission wavelength is plotted as a function of final NaTC concentration for the model bile samples of set A 24 h after mixing. Direct excitation of DL at 380 (open circle) nm yields a dansyl red shift that commences above 3 mM NaTC and continues throughout the entire NaTC concentration range. The use of 300-nm light gives indirect excitation of DL via energy transfer from DHE. Indirect excitation (solid circle) yields a dansyl blue shift that commences above 3 mM NaTC and terminates at 30 mM NaTC.

ther dansyl blue shift at NaTC concentrations exceeding 30 mM, although detection of further blue shifts would be precluded by the disappearance of the dansyl peak. Direct DL excitation at 380 nm results in an NaTC-induced increase in the dansyl emission wavelength that continues throughout the entire NaTC concentration range. The dansyl red shift reaches 30 nm at the highest NaTC loading of 87 mM.

Fluorescence spectra similar to those in Fig. 1 were measured 24 h after mixing, and Fig. 4 summarizes the 24-h spectra in terms of a fluorescence ratio, R_F . The fluorescence ratio is defined as the DHE fluorescence intensity at 373 nm divided by the maximal DL fluorescence intensity, which is wavelength dependent. Figure 4 depicts R_F as a function of NaTC concentration at an excitation wavelength of 300 nm, and NaTC-induced changes in R_F give rise to five zones, denoted as I, II, IIIa, IIIb, and IV. R_F remains constant in zone I, increases in zone II, decreases in zone IIIa, increases again in zone IIIb, and reaches a plateau in zone IV. An additional sample, at 100 mM NaTC, was made to confirm the existence of the plateau region; although drawn to coincide with sample A16, the onset of the plateau might occur at a lower NaTC concentration.

The R_F zones match the four zones that emerge from a traditional turbidity diagram. Turbidity and fluorescence were measured in samples A1–A16 simultaneously, and Fig. 4 also gives the dependence of turbidity on NaTC concentration 24 h after mixing. Turbidity was measured as absorbance at 400 nm, a wavelength at which neither fluorophore absorbs strongly, and arises from light scattering by vesicles. Turbidity remains constant in zone I, increases in zone II, decreases in zone III (a and b), and reaches a plateau in zone

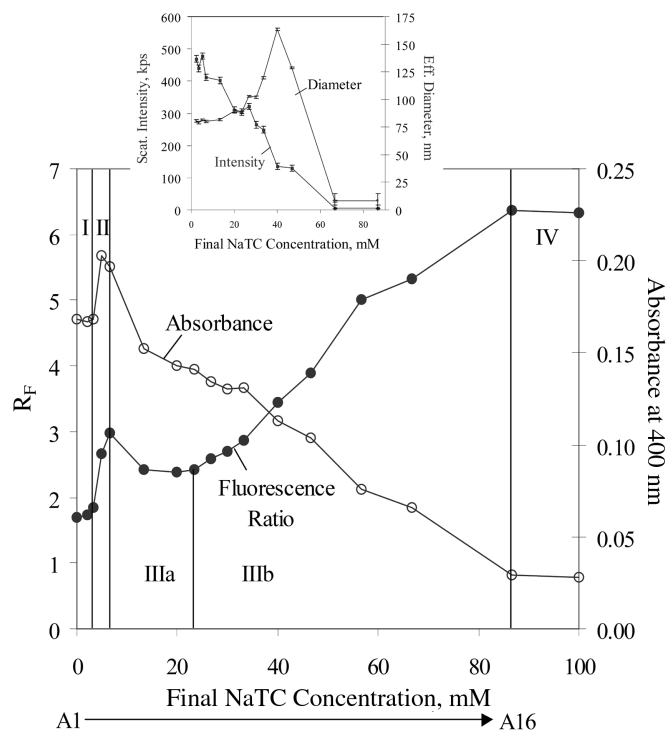


Fig. 4. The effects of NaTC concentration on turbidity (open circles), measured as absorbance at 400 nm, and fluorescence (solid circles), reported as the ratio (R_F) of DHE intensity at 373 nm to DL intensity at the maximal wavelength, are shown for samples A1–A16 24 h after mixing. Both turbidity and R_F give rise to four zones (denoted by Roman numerals) that occur at similar NaTC concentrations. The R_F trace exhibits a change in slope within zone III, which is therefore subdivided into zones IIIa and IIIb. Because absorbance does not provide any information about particle size or shape, a second set of samples with compositions matching A1–A16 was studied by dynamic light scattering. The inset figure shows scattering intensity at 90° , given as kilocounts per second (kps), and effective particle diameter, as calculated from the Stokes-Einstein equation, as a function of NaTC concentration.

IV. There is excellent agreement between the R_F zones and turbidity zones with respect to NaTC concentration. However, there is a discrepancy between R_F and turbidity within zone III; whereas turbidity decreases steadily throughout zone III, R_F exhibits both an increase and a decrease, and the subdivision of R_F zone III into zones IIIa and IIIb reflects this fact.

Also shown in Fig. 4 (inset) are the results of a dynamic light scattering experiment performed for a second set of samples that was prepared in an identical fashion to A1–A16. The light-scattering intensity, measured at a scattering angle of 90° , follows the same qualitative trend as absorbance, which is a crude measure of scattering. Dynamic light-scattering experiments indicate a steady growth of particles from 80 to 170 nm with increasing NaTC loading at intermediate NaTC loadings. This size range is typical of vesicles and suggests that the vesicles grow, presumably due to aggregation, with added bile salt. At bile salt loadings exceeding 70 mM, however, the particle size decreases dramatically and no longer varies with NaTC loading. The count rates are sufficiently low at these bile salt

loadings that accurate determination of a particle size is difficult; the particle size at each NaTC loading exceeding 70 mM falls in the range 4–13 nm, which is consistent with a population of micelles.

Because scattering intensity is proportional to the sixth power of particle size, scattering from large particles obscures scattering from small particles and complicates the identification of two coexisting particle populations. To overcome this difficulty, several samples were characterized further by fractionation on a gel filtration column. **Figure 5** shows the turbidity profile (measured as absorbance at 400 nm) as a function of fraction number for NaTC concentrations of 40 and 85 mM. Both samples exhibit two peaks, which are indicative of two particle populations, but the relative magnitudes of the two peaks vary with NaTC loading. The major peak for 40 mM NaTC appears at fraction number 9, and the particle size measured by DLS in this fraction is 196 nm, a size that is typical for vesicles. The major peak for 85 mM NaTC appears at fraction number 20, and the particle size measured by DLS in this fraction is 4–13 nm, a size that is typical for micelles. Also shown in Fig. 5 (inset) is the scattering intensity profile as a function of fraction number for the 40 mM NaTC sample, which confirms the qualitative similarity between absorbance (i.e., turbidity) and scattering intensity measurements.

The spectra of Fig. 1 suggest that R_F increases steadily with NaTC concentration. The partial decrease in the value of R_F with NaTC loading (i.e., zone IIIa in Fig. 3) stems from changes that occur during the first 24 h after mixing in samples A6–A8. **Figure 6** shows the temporal changes in R_F for five model bile samples from set A, one corresponding to each zone in Fig. 4. Samples from zone I (e.g., A1) exhibit little change in the value of R_F , and samples from

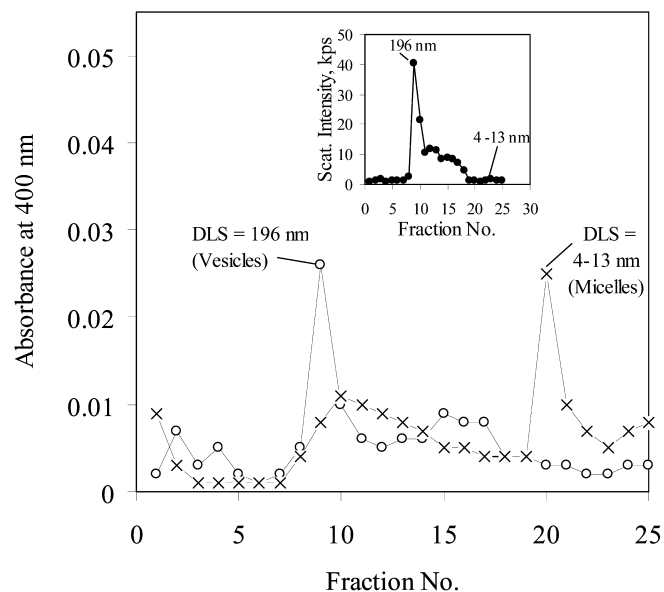


Fig. 5. Turbidity is shown as a function of fraction number for samples containing an NaTC loading of 40 (open circle) and 85 mM (X). Samples were eluted at a rate of ~ 1 ml/min on a Sephadex G-75 column with buffer containing 7.5 mM NaTC, and each fraction was 3 ml. The inset shows light-scattering intensity (kps) for the 40 mM (solid circle) sample as measured by DLS.

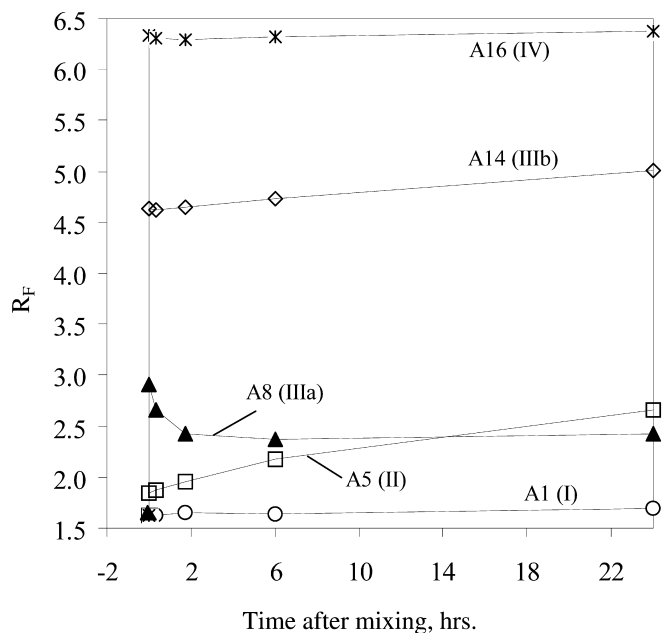


Fig. 6. The changes in R_F during the first 24 h after mixing are shown for five samples in model bile set A, one corresponding to each zone from Fig. 4. Samples from zone I (open circle) exhibit little change in R_F , and samples from zone IV (asterisk) exhibit little change in R_F after a rapid increase. Samples from zone IIIb (open diamond) exhibit a slow, steady rise in R_F after a rapid increase, and samples from zone II (open square) exhibit a continual rise in R_F with time. Zone IIIa is unique in that the R_F slope becomes negative shortly after mixing (solid triangle). The decrease in the value of R_F within zone IIIa accounts for the local minimum in the plot of R_F versus NaTC concentration (Fig. 4).

zone IV (e.g., A16) exhibit an immediate and steep, but short-lived, increase in the value of R_F with little change thereafter. Samples from zone IIIb (e.g., A14) exhibit a slight but steady increase in the value of R_F that follows an immediate, steep rise, and samples from zone II (e.g., A5) exhibit a continual increase in the value of R_F throughout the 24-h period. Zone IIIa is the only zone for which the R_F trace contains a negative slope. The samples within zone IIIa (e.g., A8) exhibit an immediate, steep increase in the value of R_F that is followed by a decrease. The decrease of R_F within zone IIIa is of sufficient magnitude that increases in the NaTC concentration, although they give initially higher values of R_F , lead to smaller R_F values at 24 h. The time-dependent decrease of R_F within zone IIIa gives rise to the local minimum in the plot of R_F versus NaTC concentration (Fig. 4).

Model biles—set B

The model biles in set B were observed for nominally 4 weeks, and **Figure 7** shows the changes in fluorescence intensities that occurred during that period. Initial intensities mimic the results of set A (Fig. 1) in that increased NaTC loadings give higher DHE intensities and lower DL intensities. Samples B1 and B2 both exhibit an increase in DHE intensity that lasts approximately 11 days, but whereas sample B2 exhibits a concomitant decrease in DL intensity, the DL intensity in sample B1 exhibits little change. The DHE and DL intensity profiles of sample B2 appear as mirror im-

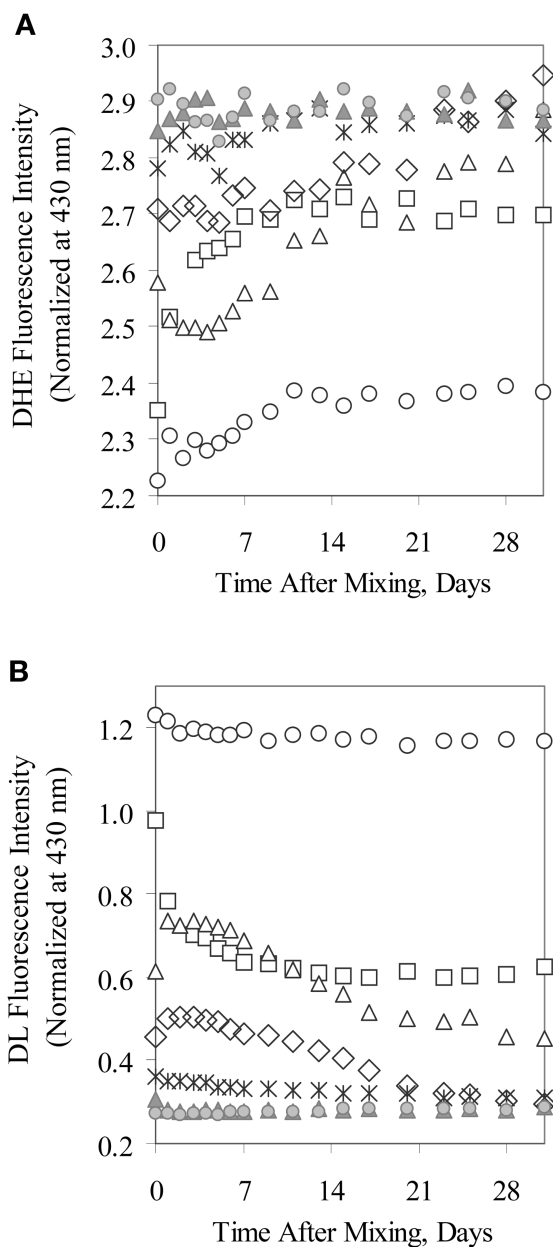


Fig. 7. Fluorescence intensities for (A) DHE at 373 nm and (B) DL at the maximal wavelength are shown as a function of time after mixing for samples B1 (open circle), B2 (open square), B3 (open triangle), B4 (open diamond), B5 (asterisk), B6 (solid triangle), and B7 (solid circle). Final NaTC concentrations were 0, 7, 27, 40, 53, 67, and 100 mM, respectively. Excitation was at 300 nm, and fluorescence intensities were normalized at an emission wavelength of 430 nm.

ages of one another, which indicate a loss of energy transfer. Similar mirror image profiles occur in samples B3–B5, and the intensities of both fluorophores remain unchanged beyond 24 h in samples B6 and B7.

Figure 8 summarizes the results of Fig. 7 in terms of the single parameter, R_F . The fluorescence ratio varies with NaTC loading in a similar fashion to that of model bile set A (Fig. 4) during the first 24 h. After Day 1, R_F exhibits no further change in samples B1 and B7, which correspond to extremes in NaTC concentration. Intermediate NaTC loadings, however, exhibit abrupt changes in the slope of

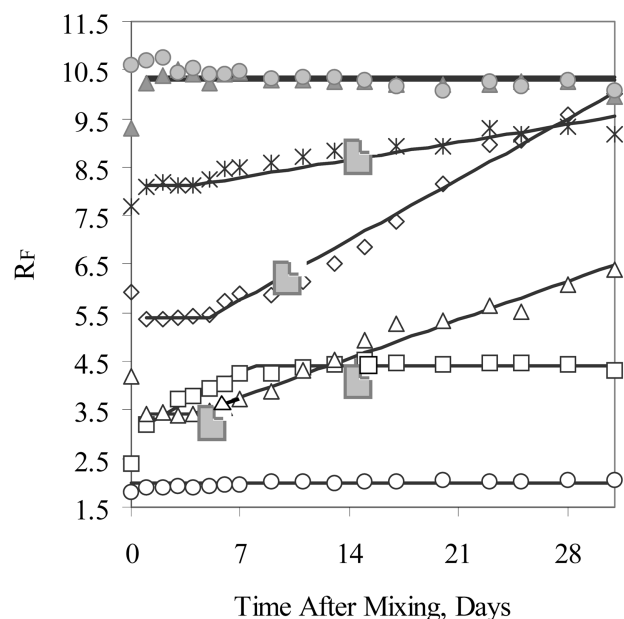


Fig. 8. The fluorescence ratio is plotted as a function of time after mixing in the model bile of set B. Symbols are identical to those in Fig. 7. Solid lines are the best piecewise-continuous fits, using the method of least squares, and notched parallelograms denote the times at which birefringent crystals first appeared in the polarizing microscope. The increase in the fluorescence ratio always precedes the appearance of microscopic cholesterol monohydrate crystals.

the R_F profile. The fluorescence ratio first remains constant and then increases in samples B3–B5. On the other hand, R_F first increases in sample B2 and remains constant thereafter.

The trends in the R_F profiles that occur after 24 h were fit with piecewise-continuous functions, shown as solid lines in Fig. 8, minimizing error by the method of least squares. According to the best fits, the increase in R_F begins on days 1, 4, 7, and 4 in samples B2, B3, B4, and B5, respectively. Each sample was observed with polarized light under the microscope, and Fig. 8 depicts the time of the earliest appearance of crystals with a symbol in the shape of a notched parallelogram. Crystals first appeared on days 14, 4, 10, and 14 in samples B2, B3, B4, and B5, respectively, and crystal appearance always superseded or, in the case of sample B3, coincided with the initial increase in R_F . No crystals were observed during the 4-week period in samples for which the fluorescence ratio did not increase (i.e., B1, B6, and B7).

Figure 9 shows the temporal changes in turbidity, measured as absorbance at 400 nm, that occurred in samples B1–B7. As with the fluorescence ratio, turbidities vary with NaTC loading in a similar fashion to that of set A during the first 24 h. After day 1, sample B1 exhibits the greatest growth in turbidity. All remaining samples exhibit a turbidity profile that appears similar to the corresponding R_F profile in Fig. 8, but the onset of the turbidity increase does not always correlate with the initial increase in the fluorescence ratio. Specifically, the rise in turbidity precedes the rise in R_F for sample B3 (day 1 vs. day 4), but the

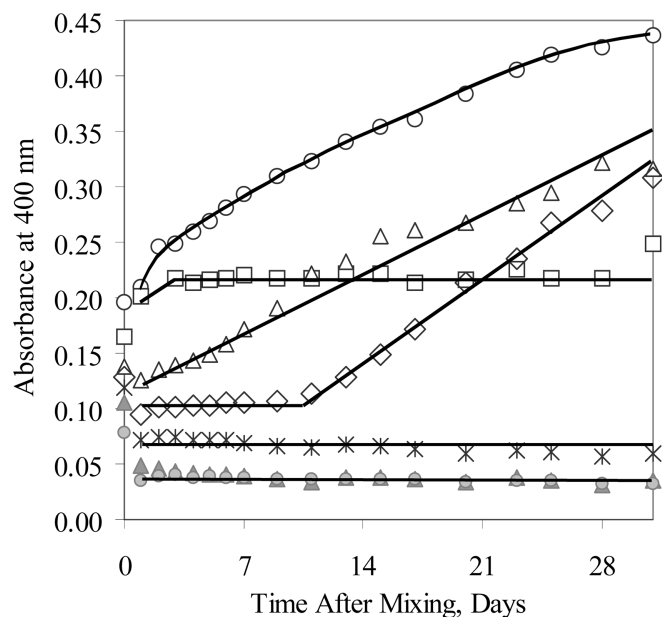


Fig. 9. Absorbance at 400 nm is plotted as a function of time after mixing in the model biles of set B. Symbols are identical to those in Figs. 7 and 8.

rise in turbidity supersedes the rise in R_F for sample B4 (day 10 vs. day 5). In the latter case the onset of turbidity coincides with the first appearance of microscopic cholesterol monohydrate crystals. **Table 3** summarizes the changes in turbidity, R_F , and crystal appearance for the samples comprising set B.

Model biles—set C

Figure 10 shows the fluorescence spectra of the model biles in set C immediately after mixing vesicles with NaTC. Similar to the observation of alleviation of energy transfer caused by NaTC in set A, a correlation between energy transfer and the sterol-to-lecithin molar ratio is observed in set C. Since DHE accounts for a larger percentage of lipids relative to dansyl (i.e., 17.5 vs. 4.5%), increasing the sterol-to-lecithin molar ratio increases the overall percentage of fluorophores. This reduces the average separation between DHE and DL and improves energy transfer.

Thus, despite having the highest DHE-to-DL molar ratio, sample C5 gives the lowest DHE fluorescence intensity and the highest DL fluorescence intensity. Likewise, sam-

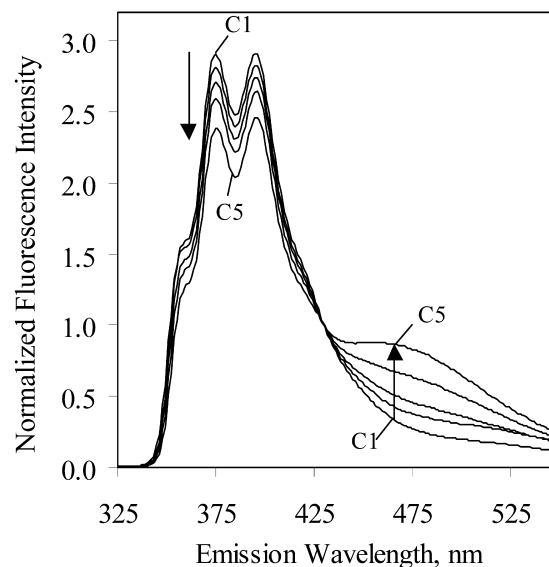


Fig. 10. The effect of increasing the sterol-to-lecithin molar ratio on DHE-to-DL energy transfer is shown for the model biles making up set C. The DHE intensity is maximal, and the DL intensity is minimal, in sample C1, which contains the lowest sterol-to-lecithin molar ratio (0.49). The increase in the sterol-to-lecithin molar ratio that accompanies the progression from samples C1 to C5 leads to a steady decrease in the DHE intensity and a concomitant steady increase in the DL intensity. This signifies an enhancement of energy transfer from DHE to DL resulting from closer proximity of the two fluorophores. Excitation was at 300 nm, and fluorescence intensities were normalized at an emission wavelength of 430 nm.

ple C1 contains the lowest DHE-to-DL molar ratio, yet exhibits the highest DHE intensity and the lowest DL intensity. The DHE intensity decreases steadily, and the DL intensity concomitantly increases, as the sterol-to-lecithin molar ratio is increased from sample C1 to C5. Note that these trends also result, at least in part, from varying degrees of micellization among the multiple cholesterol loadings. This is because higher cholesterol loadings shift the four zones (i.e., zones I–IV) in Fig. 4 to higher bile salt concentrations. Thus, micellization, and hence the increase in the fluorescence ratio, are greatest in sample C1 and least in sample C5.

The model biles of set C were also monitored for a nominally 4-week period, and **Fig. 11** shows the temporal changes in the intensities of DHE and DL. Sample C1, which is undersaturated in cholesterol, exhibits no changes in the intensity of either fluorophore. On the other hand, all supersaturated samples exhibit both an increase in the DHE intensity and a decrease in the DL intensity. The slopes of the DHE and DL profiles in each sample are opposite in sign but nearly equal in magnitude, so that the DHE and DL profiles of a given sample appear as mirror images of one another.

Increasing the sterol-to-lecithin molar ratio increases the rate of change in the intensity of both fluorophores. Moreover, the absolute changes in magnitude of both the DHE intensity and the DL intensity grow progressively as the sterol-to-lecithin molar ratio is increased. This is shown more clearly in **Fig. 12**, which gives the emission spectra in the four supersaturated samples of set C immediately and 1 month

TABLE 3. Summary of turbidity, R_F and crystal appearance—set B

Sample	Final [NaTC]	Onset of Turbidity Rise	Initial Increase In R_F	Crystal Appearance
	<i>mM</i>			
B1	0	Day 1	None	None
B2	7	Day 1	Day 1	Day 14
B3	27	Day 1	Day 4	Day 4
B4	40	Day 10	Day 7	Day 10
B5	53	None	Day 4	Day 14
B6	67	None	None	None
B7	100	None	None	None

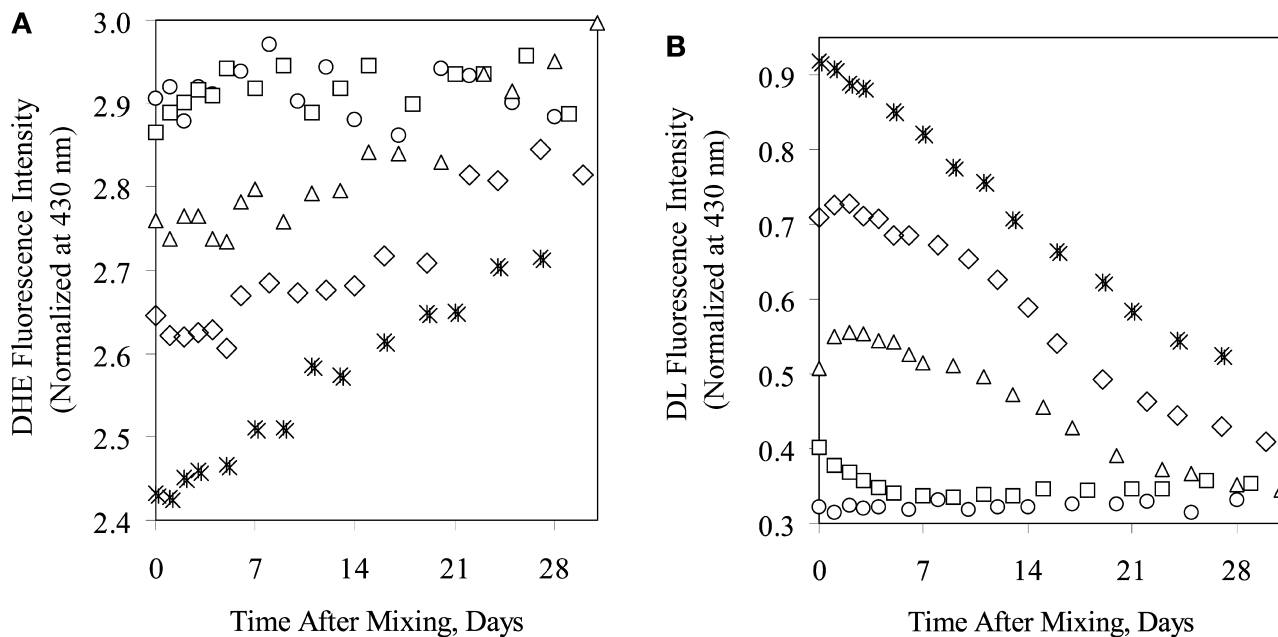


Fig. 11. Fluorescence intensities for (A) DHE at 373 nm and (B) DL at the maximal wavelength are shown as a function of time after mixing for samples C1 (open circle), C2 (open square), C3 (open triangle), C4 (open diamond), and C5 (asterisk). Sterol-to-lecithin ratios were 0.49, 1.00, 1.22, 1.50, and 1.86, respectively. Excitation was at 300 nm, and fluorescence intensities were normalized at an emission wavelength of 430 nm.

after mixing vesicles with NaTC. Small changes in intensities occur in the equimolar sample (C2), and progressively larger spectral changes occur as the sterol-to-lecithin molar ratio increases toward 1.86 (C5).

Figure 13 quantifies the changes that occurred in set C

in terms of the fluorescence ratio, R_F . Sample C1 exhibits no change in the fluorescence ratio, but samples C2–C5 exhibit abrupt changes in the slope of the R_F profile. The fluorescence ratio remains constant for nearly a week in samples C3–C5 before increasing, whereas the fluores-

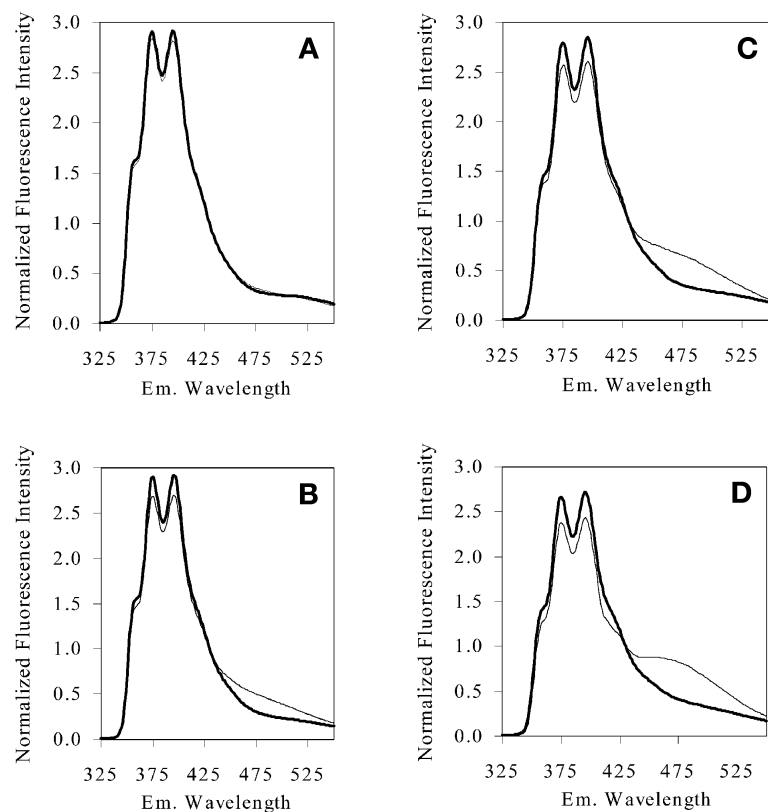


Fig. 12. Fluorescence emission spectra in samples C2–C5 are shown in panels (A)–(D), respectively. Initial spectra appear as light solid lines, and bold lines are the spectra obtained nominally 4 weeks after mixing vesicles with NaTC. Excitation was at 300 nm, and fluorescence intensities were normalized at an emission wavelength of 430 nm.

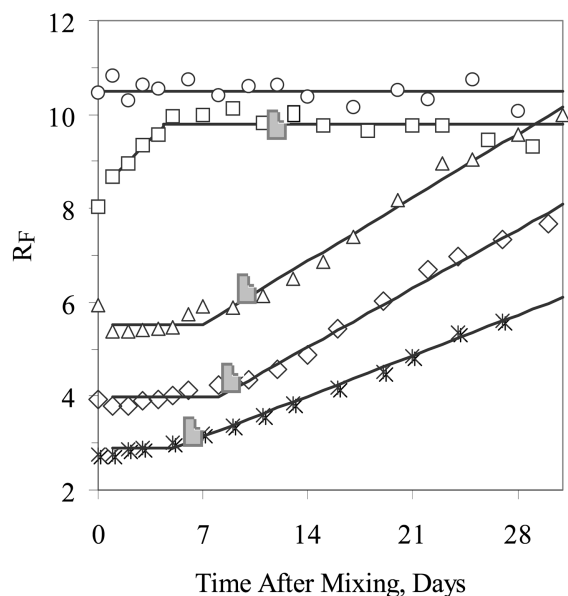


Fig. 13. The fluorescence ratio is plotted as a function of time after mixing in the model bile of set C. Symbols are identical to those in Fig. 11. Solid lines are the best piecewise-continuous fits, using the method of least squares, and notched parallelograms denote the times at which birefringent crystals first appeared in the polarizing microscope. Crystal appearance time correlates with the level of cholesterol supersaturation, and microscopic cholesterol crystals always appear after the commencement of an increase in the fluorescence ratio.

cence ratio first increases for several days in sample C2 and remains constant thereafter. The results of set C (Fig. 13) resemble those of set B (Fig. 8), and solid lines in Fig. 13, as in Fig. 8, are the best piecewise-continuous fits using a least squares regression. According to the best fits the increase in the fluorescence ratio commences on days 1, 7, 8, and 5 in samples C2, C3, C4, and C5, respectively.

Notched parallelograms in Fig. 13 denote crystal appearance times, which are 12, 10, 9, and 6 days in samples C2, C3, C4, and C5, respectively. Crystal appearance time therefore decreases with increasing cholesterol supersaturation, as expected, and no crystals were observed in the undersaturated sample (C1). Similar to the results of set B (Fig. 8), the initial increase in R_F always precedes the first appearance of crystals. Moreover, the appearance of crystals in set C always coincides with the onset of turbidity, which is shown in **Figure 14**. **Table 4** summarizes the changes in turbidity, R_F , and crystal appearance for the samples that make up set C.

DISCUSSION

The primary goal of the present work is to assess the feasibility of DHE-to-DL energy transfer as a means of measuring cholesterol nucleation kinetics in model bile. We begin by demonstrating the utility of DHE-to-DL energy transfer in characterizing lecithin-cholesterol vesicles in the presence of NaTC. First, the alleviation of energy transfer in Fig. 1 provides an alternative way of measuring the vesicle-

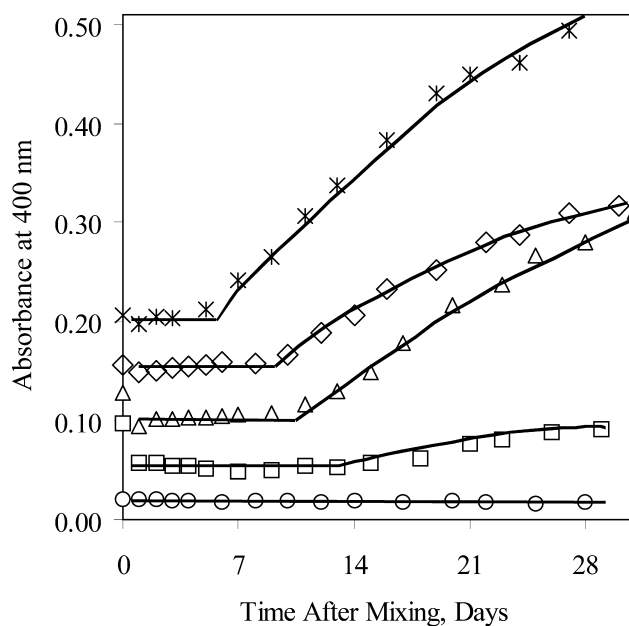


Fig. 14. Absorbance is plotted as a function of time after mixing in the model bile of set C. Symbols are identical to those in Figs. 11 and 13.

to-micelle transition in model bile. Initially, both DHE and DL reside in close proximity within the vesicle bilayer, where energy transfer proceeds readily. The reorganization of molecules into micelles, which are smaller and more numerous than the vesicles, increases the average separation between DHE and DL and alleviates energy transfer.

This claim that the changes in Fig. 1 represent micellization of vesicles is supported by several additional lines of evidence: dynamic light-scattering studies, which give scattering intensities and particle sizes consistent with both vesicles and micelles (Fig. 4); gel filtration studies, which demonstrate that vesicles and micelles coexist and that the relative proportion of micelles increases with NaTC loading (Fig. 5); and controlled fluorescence experiments, in which increasing the micellar loading in mixtures of separately prepared vesicles and micelles gives an increasing fluorescence ratio in a manner that is similar to Fig. 1 (Fig. 2).

Second, the use of both direct and indirect excitation not only confirms the coexistence of vesicles and micelles but also reveals the preferential micellization of lecithin relative to cholesterol. Whereas indirect excitation gives DL fluorescence via energy transfer from DHE and identifies only those regions where the two fluorophores reside together, direct excitation leads to additional DL fluores-

TABLE 4. Summary of turbidity, R_F and crystal appearance—set C

Sample	Ch:L	Onset of Turbidity Rise	Initial Increase In R_F	Crystal Appearance
C1	0.49	None	None	None
C2	1.00	Day 12	Day 1	Day 12
C3	1.22	Day 10	Day 7	Day 10
C4	1.50	Day 9	Day 8	Day 9
C5	1.86	Day 6	Day 5	Day 6

cence from any regions where DL might exist in the absence of DHE. If lecithin and cholesterol (and hence DHE and DL) partition evenly among vesicles and micelles, no spectral shifts would be evident. The dependence of the DL emission wavelength on excitation wavelength in Fig. 3 therefore suggests the presence of two dansyl environments, in support of vesicle/micelle coexistence. Moreover, the dansyl blue shift indicates a decrease in polarity in those regions containing both fluorophores, and the red shift indicates an increase in polarity in those regions where DL exists apart from DHE. Because an increase in the cholesterol mole fraction is known to induce dansyl blue shifts (22), these results point to cholesterol enrichment of the vesicles commensurate with micellization.

Third, quantification of the vesicle-to-micelle transition using the fluorescence ratio, R_F , potentially captures subtleties of the micellization process such as re-vesiculation. The rapid rise in R_F that occurs in sample A8 (Fig. 6) reflects an immediate alleviation of energy transfer, as would occur upon instant solubilization of vesicles by NaTC into mixed micelles. The subsequent decrease in the fluorescence ratio suggests a reversal of the micellization process and is consistent with turbidity studies that explain the reversal in terms of vesicle reformation (23). Such re-vesiculation brings DHE and DL back into close proximity and enhances energy transfer, thereby decreasing the fluorescence ratio. The results indicate that re-vesiculation occurs over the low-end range of NaTC concentrations for which vesicles and micelles coexist (i.e., zone IIIa in Fig. 4) and that the time scale for re-vesiculation is approximately 6 h.

Thus, DHE-to-DL energy transfer is at the very least a complementary technique that allows characterization of vesicle and bile salt interactions. The utility of the DHE/DL fluorescence assay stems from the sharp distance dependence ($1/d^6$) of energy transfer, which is commonly referred to as the *spectroscopic ruler* (20). Any mechanism that separates DHE and DL also alleviates energy transfer and leads to a measurable rise in the DHE fluorescence intensity and a concomitant fall in the DL fluorescence intensity. One such mechanism is certainly the micellization process already mentioned, which alleviates energy transfer within 24 h as an increasing function of bile salt loading. Nucleation of cholesterol (and DHE) out of the vesicles is a second mechanism that would alleviate energy transfer, and we now explore the potential of DHE-to-DL energy transfer as an assay for measuring cholesterol nucleation in model bile.

When the NaTC loading is insufficient to give total micellization, the ensuing micellization provides only partial alleviation of energy transfer, and residual DHE-to-DL energy transfer proceeds with finite efficiency in the remaining cholesterol-enriched vesicles. This explains the initial correlation between the fluorescence ratio and NaTC loading on day 0 and day 1 in model bile set B (Fig. 7). In particular, partial micellization accounts for the intermediate values of R_F at intermediate NaTC loadings similar to the results of Fig. 4. Since the vesicle-to-micelle transition is complete within 24 h, cholesterol nucleation from vesicles at intermediate bile salt loadings should lead to a

time-dependent increase in the fluorescence ratio beyond the initial increase associated with micellization.


The existence of a time-dependent increase in the fluorescence ratio for each intermediate NaTC loading in set B (Fig. 8) suggests that DHE-to-DL energy transfer is indeed a reporter of cholesterol nucleation. The fact that R_F does not increase in sample B7, which contains only mixed micelles and cannot nucleate cholesterol, is consistent with that claim. Sample B1 also supports the claim that increases in R_F result from cholesterol nucleation by ruling out vesicle aggregation and/or fusion as a possible cause. This is because sample B1 exhibits extensive vesicle aggregation and fusion, as observed in the microscope and via turbidity measurements (Fig. 9), yet exhibits no increase in the fluorescence ratio within the 4-week observation period.

Further evidence that DHE-to-DL energy transfer is a reporter of nucleation is the fact that the initial increase in the fluorescence ratio always precedes the appearance of microscopic cholesterol crystals. Moreover, the increase in R_F occurs after a lag period, which is consistent with classical nucleation theory. The lag period is also consistent with video-enhanced microscopy studies, which indicate that cholesterol nucleation/crystallization occurs only after substantial vesicle aggregation and fusion (24). This may explain why the initial increase in the fluorescence ratio occurs earliest in sample B2, which contains the lowest vesicular cholesterol-to-lecithin ratio. Increasing the NaTC loading in set B increases the micellar fraction at the expense of decreasing the number density of vesicles. Thus, sample B1 contains only vesicles, sample B7 contains no vesicles, and samples B2–B6 contain decreasing number densities of vesicles in the order $B2 > B3 > B4 > B5 > B6$. One thus expects the rates of vesicle aggregation and fusion to be maximal in sample B1 and to decrease progressively with increased NaTC loading. Nucleation may therefore occur earliest in sample B2 as a result of faster rates of vesicle aggregation and fusion.

Conversely, the vesicle fraction is sufficiently small in samples with higher NaTC loadings that vesicle aggregation and fusion cause no measurable increase in turbidity. The onset of turbidity in sample B4 coincides with crystal appearance, and the increase in turbidity likely reflects crystal growth. Between these extremes, vesicle aggregation causes a rise in turbidity that precedes the initial rise in the fluorescence ratio, and the fluorescence ratio increases prior to the first appearance of microscopic cholesterol crystals. Thus, the time scales of the fluorescence intensity changes, and the correlation of the changes with NaTC loading, are consistent with a mechanism of cholesterol nucleation. These changes are also consistent with a mechanism of lateral phase separation of cholesterol within the vesicle bilayer, but the eventual appearance of crystals in all samples for which the fluorescence ratio increases suggests that any lateral phase separation is transient.

Model bile set C lends further support to the use of DHE-to-DL energy transfer as an assay for measuring cholesterol nucleation. Fig. 10 shows that the extent of energy transfer from DHE to DL decreases as the cholesterol mole fraction of the starting vesicles is lowered. Since cholesterol nucleation reduces the cholesterol mole fraction in the vesicle

phase, one expects a similar alleviation of energy transfer with time as nucleation proceeds. Fig. 11 shows that a time-dependent alleviation of energy transfer occurs in each supersaturated model bile of set C (samples C2–C5) but not for the undersaturated sample (C1). The rates of change of the individual fluorescence intensities, as well as the magnitudes of the changes, increase with cholesterol loading. Thus, by the end of the 4-week observation period sample C2 gives an almost imperceptible change in fluorescence emission spectra, and fluorescence changes are most prevalent for sample C5 (Fig. 12). DHE-to-DL energy transfer therefore provides a measure of the rate of cholesterol nucleation, revealing that nucleation proceeds more rapidly, and to a greater extent, as the cholesterol supersaturation is increased. As in model bile set B, the fluorescence ratios in the supersaturated samples of set C exhibit an abrupt change in slope that always precedes the first appearance of microscopic crystals (Fig. 13). R_F is therefore also useful as a marker for the onset of nucleation.

To summarize, we have utilized a fluorescence assay based on energy transfer from DHE to DL to examine lecithin-cholesterol vesicles in the presence of the bile salt, NaTC. The assay gives agreement with a conventional technique with respect to characterization of the vesicle-to-micelle transition, revealing both the preferential micellization of lecithin (relative to cholesterol) and the process of re-vesiculation. More important, the fluorescence assay reveals an alleviation of DHE-to-DL energy transfer that occurs beyond the time scales for vesicle aggregation and fusion and prior to the appearance of microscopic crystals. The rate and extent of the loss in energy transfer correlate with cholesterol supersaturation, and the assay gives results that are consistent with a mechanism of cholesterol nucleation. The model bile solutions in this work contain near physiological lipid concentrations, and the DHE-to-DL energy transfer fluorescence assay should prove useful in characterizing the kinetic effects of the putative pro- and anti-nucleating factors in native bile. 

This work was supported in part by Grant R01 DK41678 from the National Institutes of Health and a VA Merit Review Award. Sum P. Lee is supported in part by the Medical Research Service of the Department of Veterans Affairs.

Manuscript received 11 February 2000, in revised form 9 August 2000, and in re-revised form 22 December 2000.

REFERENCES

- Holzbach, R. T., M. Marsh, M. Olszewski, and K. Holan. 1973. Cholesterol solubility in bile—evidence that supersaturated bile is frequent in healthy man. *J. Clin. Invest.* **52**: 1467–1479.
- Small, D. 1980. Cholesterol nucleation and growth in gallstone formation. *N. Engl. J. Med.* **302**: 1305–1307.

- Holan, K. R., R. T. Holzbach, R. E. Hermann, A. M. Cooperman, and W. J. Claffey. 1979. Nucleation time: A key factor in the pathogenesis of cholesterol gallstone disease. *Gastroenterology*. **77**: 611–617.
- Somjen, G. T., and T. Gilat. 1983. A non-micellar mode of cholesterol transport in human bile. *FEBS Lett.* **156**: 265–268.
- Hofmann, A. F. 1990. Bile acid secretion, bile flow and biliary lipid secretion in humans. *Hepatology*. **12**: 17S–22S.
- Carey, M. C., and J. T. Lamont. 1992. Cholesterol gallstone formation. 1. Physical-chemistry of bile and biliary lipid secretion. *Prog. Liver Dis.* **10**: 139–163.
- Somjen, G., and T. Gilat. 1985. Contribution of vesicular and micellar carriers to cholesterol transport in human bile. *J. Lipid Res.* **26**: 699–704.
- Carey, M. C. 1978. Critical tables for calculating the cholesterol saturation of native bile. *J. Lipid Res.* **19**: 945–955.
- Kibe, A., M. A. Dudley, Z. Halpern, M. P. Lynn, A. C. Breuer, and R. T. Holzbach. 1985. Factors affecting cholesterol monohydrate crystal nucleation time in model bile systems of supersaturated bile. *J. Lipid Res.* **26**: 1102–1111.
- Lee, S. P., J. T. Lamont, and M. C. Carey. 1981. Role of gallbladder mucus hypersecretion in the evolution of cholesterol gallstones—studies in the prairie dog. *J. Clin. Invest.* **67**: 1712–1723.
- Levy, P. R., B. F. Smith, and J. T. LaMont. 1984. Human gallbladder mucin accelerates nucleation of cholesterol in artificial bile. *Gastroenterology*. **87**: 270–275.
- Kibe, A., R. T. Holzbach, N. F. LaRusso, and S. J. T. Mao. 1984. Inhibition of cholesterol crystal formation by apolipoproteins in supersaturated model bile. *Science*. **25**: 514–516.
- Busch, N., H. Tokumo, and R. T. Holzbach. 1990. A sensitive method for determination of cholesterol growth using model solutions of supersaturated bile. *J. Lipid Res.* **31**: 1903–1909.
- Pattinson, N. R., and K. E. Willis. 1991. Nucleation of cholesterol crystals from native bile and the effect of protein hydrolysis. *J. Lipid Res.* **32**: 215–221.
- Busch, N., N. Matiuck, S. Sahlin, S. P. Pillay, and R. T. Holzbach. 1991. Inhibition and promotion of cholesterol crystallization by protein fractions from normal human gallbladder bile. *J. Lipid Res.* **32**: 695–702.
- Tazuma, S., H. Ochi, K. Horikawa, H. Miura, T. Ohya, G. Kajiyama, and K. Itoh. 1995. Effect of phospholipid fatty acid composition on cholesterol nucleation and crystal growth. *Bile Acids in Gastroenterology*. **80**: 315–318.
- Angelico, M., A. Nistri, P. D. Guardia, and L. Baiocchi. 1995. Cholesterol transport and nucleation in bile. In *Methods Biliary Research*; M. Muraca, editor. Boca Raton, FL, pp. 65–80.
- Wang, D. Q.-H., and M. C. Carey. 1996. Complete mapping of crystallization pathways during cholesterol precipitation from model bile: influence of physical-chemical variables of pathophysiologic relevance and identification of a stable liquid crystalline state in cold, dilute and hydrophobic bile salt-containing systems. *J. Lipid Res.* **37**: 606–630.
- Yamashita, Y., S. Tazuma, and G. Kajiyama. 1996. Method for quantitative assessment of transformation of non-micellar cholesterol carriers in model bile systems. *J. Gastroenterol. Hepatol.* **11**: 864–869.
- Stryer, L. 1978. Fluorescence energy transfer as a spectroscopic ruler. *Annu. Rev. Biochem.* **47**: 819–846.
- Kim, Y. S., A. S. Luk, E. W. Kaler, and S. P. Lee. 1994. *Gastroenterology*. **106**: A343 (Abstract).
- Wrenn, S., E. W. Kaler, and S. P. Lee. 1999. A fluorescence energy transfer study of lecithin-cholesterol vesicles in the presence of phospholipase C. *J. Lipid Res.* **40**: 1483–1494.
- Lichtenberg, D., S. Ragimova, A. Bor, S. Almog, C. Vinkler, M. Kalina, Y. Peled, and Z. Halpern. 1988. Stability of mixed micellar bile models supersaturated with cholesterol. *Biophys. J.* **54**: 1013–1025.
- Halpern, Z., M. A. Dudley, A. Kibe, M. P. Lynn, A. C. Breuer, and R. T. Holzbach. 1986. Rapid vesicle formation and aggregation in abnormal human biles—a time-lapse video-enhanced contrast microscopy study. *Gastroenterology*. **90**: 875–885.